doi:10.1038/nature08921

LETTERS

Crystal structure of the FTO protein reveals basis for its substrate specificity

Zhifu Han[1]*, Tianhui Niu[1,2]*, Junbiao Chang[3], Xiaoguang Lei[1,4], Mingyan Zhao[1], Qiang Wang[3], Wei Cheng[1], Jinjing Wang[1], Yi Feng[1] & Jijie Chai[1,5]

Recent studies[1–5] have unequivocally associated the fat mass and obesity-associated (*FTO*) gene with the risk of obesity. *In vitro* FTO protein is an AlkB-like DNA/RNA demethylase with a strong preference for 3-methylthymidine (3-meT) in single-stranded DNA or 3-methyluracil (3-meU) in single-stranded RNA[6–8]. Here we report the crystal structure of FTO in complex with the mononucleotide 3-meT. FTO comprises an amino-terminal AlkB-like domain and a carboxy-terminal domain with a novel fold. Biochemical assays show that these two domains interact with each other, which is required for FTO catalytic activity. In contrast with the structures of other AlkB members, FTO possesses an extra loop covering one side of the conserved jelly-roll motif. Structural comparison shows that this loop selectively competes with the unmethylated strand of the DNA duplex for binding to FTO, suggesting that it has an important role in FTO selection against double-stranded nucleic acids. The ability of FTO to distinguish 3-meT or 3-meU from other nucleotides is conferred by its hydrogen-bonding interaction with the two carbonyl oxygen atoms in 3-meT or 3-meU. Taken together, these results provide a structural basis for understanding FTO substrate-specificity, and serve as a foundation for the rational design of FTO inhibitors.

Obesity is a leading cause of preventable illness and death worldwide. Genome-wide association studies[1,2] have shown a strong correlation of a single nucleotide polymorphism in the first intron of the *FTO* gene with increased body mass index and obesity risk. Mouse model studies demonstrated that FTO is functionally involved in energy homeostasis[3] and affects the whole body metabolism[4], establishing a mechanistic link between FTO and obesity. FTO protein was predicted[6,7] and biochemically confirmed[6,8] to belong to the AlkB[9,10] family of Fe^{2+}/2-oxoglutarate-dependent oxidative DNA/RNA demethylases. A link between FTO demethylase activity and increased fat mass was suggested by the observation that the single mutation Ile367Phe in mouse FTO protein with an impaired activity resulted in a lean phenotype of mouse[4]. *In vitro*, FTO strongly prefers 3-meT in single-stranded (ss)DNA[6,8] or 3-meU in ssRNA[8] as substrates, but shows no detectable activity towards double-stranded (ds)DNA or dsRNA. AlkB[9,10] and its human homologues ABH1 (also known as ALKBH1)[11] and ABH3 (ALKBH3)[12–14] share the ability to demethylate 1-methyladenine (1-meA) and 3-methylcytosine (3-meC) in DNA/RNA. The significance of RNA demethylation by AlkB has been demonstrated *in vivo*[12,15]. Although ABH2 shows similar nucleotide specificity to these three proteins, it was found to be markedly more active on dsDNA than on ssDNA[12,13]. By contrast, ABH1 and ABH3 strongly prefer ssDNA/RNA as substrates[11–13], whereas AlkB has a slightly higher activity towards single-stranded than double-stranded nucleic acids[9,10]. Structural[16–19] and biochemical[11,20] studies have provided much information on the substrate-selection mechanisms of the four proteins. However, it remains unknown how FTO selectivity is achieved.

To investigate the mechanism underlying FTO substrate selection, we determined the crystal structure of human FTO with an N-terminally truncated 31 residues (FTOΔ31) bound by the mononucleotide 3-meT, which was used as an FTO substrate in previous studies[21,22]. Deletion of the N-terminal 31 residues had no effect on FTO catalytic activity (Supplementary Fig. 1). *N*-oxalylglycine (NOG) was used for formation of a catalytically inert FTO–substrate complex. The final model of the FTOΔ31–3-meT complex was refined to 2.5 Å resolution (Supplementary Table 1).

In crystal, a trimer related by crystallographic three-fold symmetry is mainly mediated by Trp 278 (Supplementary Fig. 2). However, the mutation Trp278Asp had no effect on its position under gel-filtration assay and its enzymatic activity (data not shown), indicating that such a trimer resulted from crystal packing. The structure of FTOΔ31 contains two well-defined domains: an N- (residues 32–326) and a C- (residues 327–498) terminal domain (referred to as NTD and CTD, respectively). As predicted[6,7], the catalytic core of the NTD is mainly composed of a distorted double-strand β-helix (Fig. 1, β5−β12) dubbed as a jelly-roll motif[23]. One side of the jelly-roll motif is buttressed by two α-helices (α3 and α4), whereas the other side is covered by a long loop linking β5 and β6 (Fig. 1). In agreement with previous modelling studies[6,7], the highly conserved residues His 231, Asp 233 and His 307 (Supplementary Fig. 3) are coordinated to Fe^{2+}. In addition to chelating Fe^{2+}, NOG also forms salt bonds with Arg 316 and Arg 322 (Supplementary Fig. 4).

No known structure was identified to share significant homology with the CTD, indicating that it represents a new fold. Consistent with the circular dichroism spectroscopy study[4], the CTD is primarily α-helical, with α7, α8 and α10 forming a three-helix bundle (Fig. 1). One end of the helix bundle makes extensive interactions with the NTD (Fig. 2a), suggesting that the CTD has an important role in stabilizing the conformation of the NTD. Consistently, the mutations Phe114Asp or Cys392Asp that are expected to perturb the NTD–CTD interaction (Fig. 2b, c) greatly reduced FTO activity (Fig. 2d). Furthermore, although the NTD was enzymatically inactive (Fig. 2d) when expressed alone, its co-expression with the CTD in *Escherichia coli* resulted in formation of a stable complex (Fig. 2c) and partially rescued the activity of the NTD towards 3-meT (Fig. 2d), supporting the idea that the CTD has a crucial involvement in FTO catalytic activity. Interestingly, Ile 370—the equivalent of Ile 367 in mouse FTO (Supplementary Fig. 3)—is completely buried in the structure (Supplementary Fig. 5), indicating that this residue is unlikely to be involved in FTO homodimerization as previously proposed[4]. An

[1]National Institute of Biological Sciences, No. 7 Science Park Road, Beijing 102206, China. [2]College of Biological Sciences, China Agricultural University, Beijing 100094, China. [3]Department of Chemistry, Zhengzhou University, Zhengzhou 450001, China. [4]School of Pharmaceutical Science and Technology, Tianjin University, Tianjin 300072, China. [5]Department of Biological Sciences and Biotechnology, Tsinghua University, Beijing 100084, China.
*These authors contributed equally to this work.

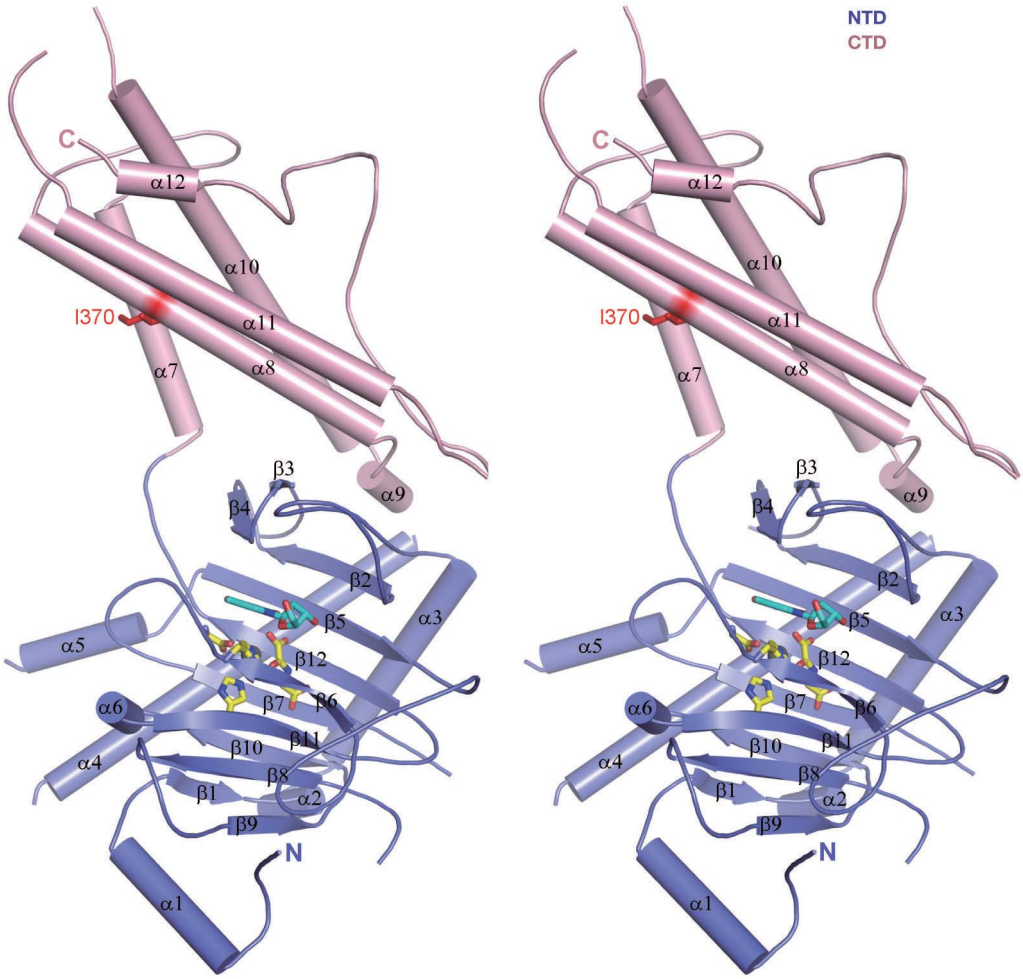

Figure 1 | FTO contains two well-defined domains. Stereo view of the overall structure of FTO. The NTD (residues 32–326) and CTD (residues 327–498) of FTO are coloured in slate and pink, respectively. The α-helices are shown in cylinder. Residue Ile 370 (red stick) corresponds to Ile 367 of mouse FTO. Fe^{2+} (grey sphere), its coordinating residues (yellow stick) and 3-meT (cyan stick) are shown.

impaired activity of the FTO mutant protein Ile367Phe may result from a change in the size of this residue, thus disturbing the conformation of the CTD and leading to a destabilized NTD.

A database search using DALI (http://www2.ebi.ac.uk/dali) showed that AlkB is the most similar structural homologue of the NTD, with a root mean squared deviation (r.m.s.d.) of 2.3 Å over 182 Cα atoms. In addition to AlkB, the structures of human ABH2 and ABH3 can also be well superimposed with that of the NTD, particularly around the central jelly-roll motif (Fig. 3a). The nucleotide recognition lid[16] is less conserved among these four proteins (Supplementary Fig. 6), but the more notable structural difference is observed at the outer wall of one side (Fig. 3a, defined by β6, β11, β8 and β9) of the jelly-roll motif. In AlkB, ABH2 and ABH3, this region is highly exposed and positively charged (Supplementary Fig. 7). By contrast, FTO possesses a further long loop (Fig. 3a, referred to as the L1 loop hereafter) that completely covers this region, making it less positively charged (Supplementary Fig. 7). Supporting the structural observation, primary sequence alignment indicates that the amino acid residues within the L1 loop are insertions compared to other AlkB members, but highly conserved among FTO proteins from different species (Fig. 3b and Supplementary Fig. 3). Interaction of the L1 loop with the jelly-roll motif is mainly mediated through Trp 230-centred hydrophobic contacts (Supplementary Fig. 8).

The superposition of AlkB– and ABH2–dsDNA complexes onto the NTD of FTO demonstrates that the L1 loop, but not any other structure element, severely clashes with the unmethylated strand of the DNA duplex, whereas the methylated strand can be modelled into the active site of FTO without steric hindrance (Fig. 3c). Thus, FTO seems to have evolved a stretch of residues that selectively blocks the unmethylated strand of dsDNA/RNA from gaining access to the substrate-binding site. A role for the L1 loop in FTO selection against dsDNA/RNA supports a previous proposal[24] that suggests that structure elements other than the region surrounding Phe 102 in human ABH2 (important in ABH2 preference for dsDNA over ssDNA[18]) can also contribute to substrate specificities of AlkB family proteins. The absence of the corresponding residue in FTO might also contribute to its selective disadvantage for dsDNA/RNA, but it does not seem to have a determining role in this process. FTO resembles human ABH1 (ref. 11) and ABH3 (refs 12–14) in that they are all ssDNA/RNA-selective. Distinct mechanisms, however, are probably used for selection against dsDNA/RNA substrates, owing to the lack of the L1 loop in the latter two.

The bound 3-meT, in particular the thymine portion, is well defined in the electron density map (Fig. 4a), and deeply anchored in a narrow substrate recognition cleft of FTO (Fig. 4b, c). The orientation of 3-meT is consistent with that of 1-meA bound in AlkB[16] (Fig. 4d). The methyl group at C5-3-meT, which is lacking in uracil and is the only difference between uracil and thymine, does not contribute to binding of 3-meT to FTO. This probably explains the observation that FTO has a similar activity towards 3-meU in ssRNA[8]. The recognition of 3-meT by FTO is through a combination of hydrogen bonds and van der Waals contacts. Similar to the 1-meA interaction with AlkB[16], the nucleobase ring of 3-meT is sandwiched between the side chains of two highly conserved residues, Tyr 108 and His 231 (Fig. 4c). Hydrophobic interaction also stems from the

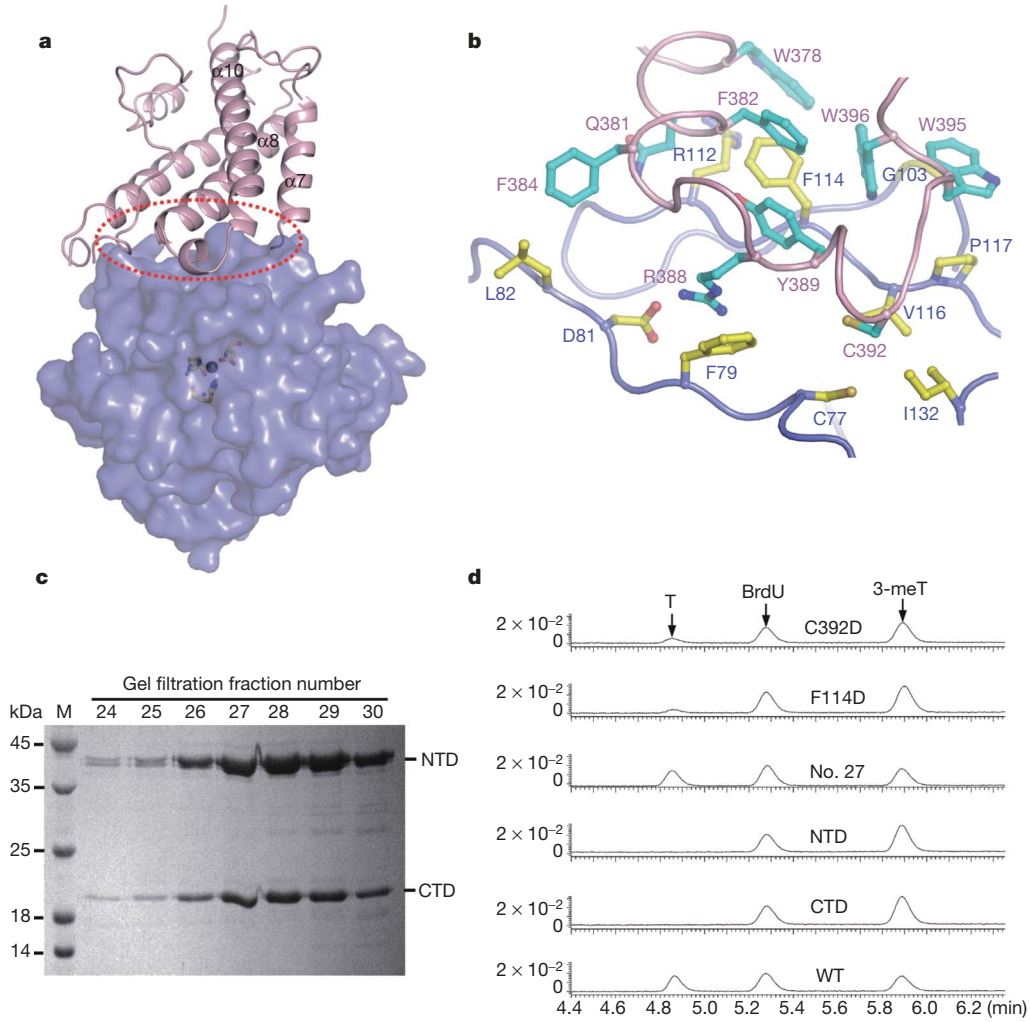

Figure 2 | Interaction between the NTD and CTD of FTO. a, The NTD (shown in surface) and the CTD (shown in cartoon) of FTO form an extensive interface as highlighted by a red dashed ellipse. Fe^{2+} (grey sphere) and its coordinating residues (yellow stick) are shown. **b**, Detailed interactions around the region highlighted in **a**. The side chains from NTD and CTD are labelled in slate and pink, respectively. **c**, The NTD (residues 1–326) and CTD (residues 327–505) form a stable complex. Samples from relevant fractions of gel filtration were applied to SDS–PAGE and visualized by Coomassie blue staining. The assay was performed as described in Methods. M, molecular mass marker. **d**, The NTD–CTD interaction is important for FTO catalytic activity. 3-meT was incubated with various FTO proteins as indicated and the reaction products were monitored by liquid chromatography–mass spectrometry (LC–MS). 'No. 27' represents the protein fraction 27 shown in **c**. The horizontal and vertical axes represent retention time (min) and ultraviolet absorbance (at 266 nm), respectively. T denotes the demethylated product of 3-meT; BrdU represents the internal standard 5-bromo-2′-deoxyuridine. About 42% of 3-meT was demethylated by wild-type FTO (Supplementary Fig. 9).

packing of Leu 109 and Val 228 against the sugar ring of 3-meT. Three hydrogen bonds contribute to the 3-meT interaction with FTO. In addition to the 1-carboxylate of NOG, O2-3-meT also forms a hydrogen bond with the conserved Arg 96 that is stabilized by Tyr 108 and Asn 205 (Fig. 4c). The significance of this hydrogen bond was verified by mutation of this residue to its equivalents in AlkB (Met 61) and ABH2 (Gln 112), which nearly abolished FTO activity (Fig. 4e). Interestingly, the naturally occurring FTO mutation Arg96His in human also resulted in loss of FTO demethylase activity[21]. The third hydrogen bond is made between the amide nitrogen of Glu 234 and O4-3-meT (Fig. 4c). Supporting the role of this hydrogen bond in FTO catalytic activity, the mutation of Glu 234 to the *cis*-proline predicted to alter its peptide orientation and thereby disrupt its hydrogen bond with the O4-3-meT, resulted in no detectable FTO activity of demethylating 3-meT (Fig. 4e).

Our current structural data provide an explanation for the preference of FTO for thymine or uracil over other nucleobases. Of all the possible contacts made to FTO, the hydrogen bond formed with Glu 234 is the only one that would be different between 3-meT and 3-meC in the nucleobase ring. Consistently, biochemical studies showed that FTO has a strong preference towards 3-meT over 3-meC[6,8]. Structural alignment revealed that O2- and O4-3-meT reside in similar positions to C2- and N6-1-meA bound in AlkB[16], respectively (Fig. 4d). Thus, interactions of these two positions of 1-meA with FTO (Fig. 2d) would be repulsive. In particular for 1-methylguanine (1-meG), introduction of an amine group at C2 would greatly increase the steric hindrance and generate an extra electrostatic repulsion, thus making 1-meG a poor substrate of FTO[6,8]. As N6-1-meA bound in AlkB is positioned in a similar region to O4-3-meT in FTO, its topological equivalent, O6-1-meG, in principle can also form a hydrogen bond with Glu 234. However, such a positioning of 1-meG in FTO, as mentioned earlier, would generate steric clashes with Arg 96, thus promoting its rejection from the active site of FTO. Collectively, our data indicate that specific hydrogen-bonding interactions with substrates contribute to FTO selection of different methylated nucleobases. Such a mechanism is reminiscent of the recognition of flipped-out uracil by uracil-DNA glycosylase[25,26].

The data presented here provide structural evidence to support the notion that FTO can act as a DNA/RNA demethylase for its functions. Because FTO localizes to cellular nucleus[6], it is conceivable that it might be involved in maintaining the integrity of the single-stranded regions of nuclear DNA/RNA. A similar role has been suggested for

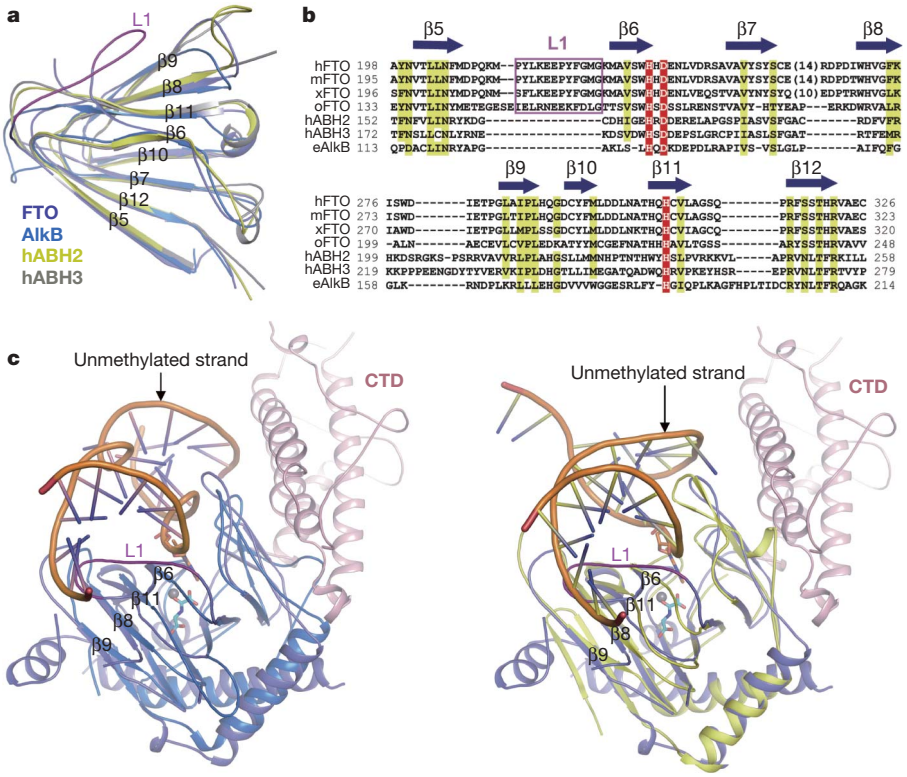

Figure 3 | An extra loop of FTO is probably important for its selection against dsDNA. **a**, Structural comparison of FTO with AlkB, human ABH2 and ABH3 around the jelly-roll motif. The extra loop L1 (residues 213–224) from FTO is shown in purple. **b**, Structure-based sequence alignment of FTO and AlkB family proteins within the jelly-roll motif. Fe^{2+}-coordinated residues are highlighted in red. e, *E. coli*; h, *Homo sapiens*; m, *Mus musculus*; o, *Ostreococcus lucimarinus*; x, *Xenopus laevis*. **c**, Structural alignments of FTO with AlkB (left) and ABH2 (right) –dsDNA complexes. 1-meA from the methylated strand of dsDNA is shown in orange stick; NOG is shown in cyan stick.

ABH3 (ref. 12). Thus, it seems that FTO, ABH3 and probably other human AlkB homologues, with distinct substrate specificities, constitute a family protein to alleviate deleterious effects of nuclear DNA/RNA methylation. It is noteworthy that 3-meT is less prevalent than 1-meA and 3-meC[24]. Given that RNA (in particular ribosomal RNA) is abundant in cells and is mainly single-stranded, it may be reasonable to assume that RNA is the primary substrate of FTO. Of particular relevance to this hypothesis is the observation that 3-meU in rRNA was found to be position-specific and can be introduced *in vitro*[27]. Furthermore, 3-meU considerably affects rRNA structure[28] and renders rRNA super sensitive to chemical cleavage[29]. The naturally occurring 3-meU has been detected in 28S rRNA of HeLa cells[30].

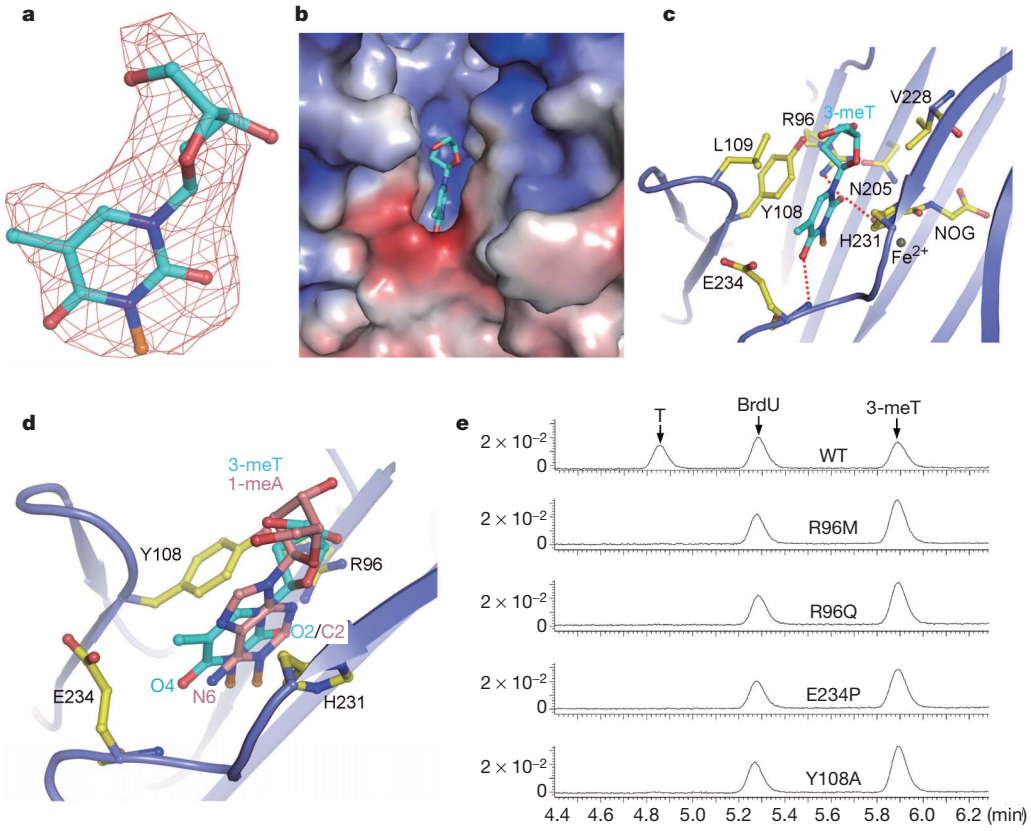

Figure 4 | Specific recognition of 3-meT by FTO. **a**, Omit electron density around 3-meT the in FTOΔ31–3-meT complex. The methyl group at N3-3-meT is coloured orange. **b**, 3-meT binds to a deep pocket on the surface of FTO (represented by electrostatic surface). **c**, Detailed interaction between FTO and 3-meT. **d**, Superposition of FTOΔ31–3-meT and AlkB–1-meA. For clarity, only 1-meA from the AlkB–1-meA complex is shown. **e**, Mutations of the 3-meT-interacting residues greatly compromise FTO demethylase activity *in vitro*. The assay was performed as described in Fig. 2d.

Thus it is tempting to speculate that demethylation of 3-meU by FTO (if it is indeed a substrate of FTO *in vivo*) might be involved in regulation of the functions/half-life of rRNA.

Our current results indicate that the single nucleotide 3-meT/3-meU contains all the essential structural determinants for FTO to recognize its substrates as observed in AlkB[16,20]. It is very likely that the nucleotides immediately flanking the methylated one also have a role in the optimal activity of FTO. Future studies are needed to determine how they contribute to substrate recognition by FTO. Nevertheless, our structural information provides a starting point for the successful development of FTO inhibitors that holds promise for developing therapeutic agents to treat obesity or even diabetes.

METHODS SUMMARY

Wild-type and various mutant human FTOs cloned into pET-15b (Novagen) were expressed in *E. coli* strain BL21(DE3). The soluble fraction of FTO was purified using an affinity column and further cleaned by an anion-exchange column. Size-exclusion chromatography was used to detect the interaction between the N- (residues 1–326) and C- (residues 327–505) terminal domain of FTO. Samples from relevant fractions were applied to SDS–PAGE and visualized by Coomassie blue staining. FTO activity was assayed using high-pressure liquid chromatography (HPLC) to monitor the reaction products as previously described[6,8]. Crystals of the FTOΔ31–3-meT complex were grown using hanging drop vapour diffusion method. Data sets for crystals of native and selenium-substituted FTO were collected at Photon Factory using a charge coupled device (CCD) detector. The FTOΔ31–3-meT structure was determined using single wavelength anomalous dispersion (SAD) method and refined with the program CNS (crystallography and NMR system) (Supplementary Table 1).

Full Methods and any associated references are available in the online version of the paper at www.nature.com/nature.

Received 27 October 2009; accepted 11 February 2010.
Published online 7 April 2010.

1. Frayling, T. M. *et al.* A common variant in the *FTO* gene is associated with body mass index and predisposes to childhood and adult obesity. *Science* **316,** 889–894 (2007).
2. Dina, C. *et al.* Variation in *FTO* contributes to childhood obesity and severe adult obesity. *Nature Genet.* **39,** 724–726 (2007).
3. Fischer, J. *et al.* Inactivation of the *Fto* gene protects from obesity. *Nature* **458,** 894–898 (2009).
4. Church, C. *et al.* A mouse model for the metabolic effects of the human fat mass and obesity associated *FTO* gene. *PLoS Genet.* **5,** e1000599 (2009).
5. Speakman, J. R., Rance, K. A. & Johnstone, A. M. Polymorphisms of the *FTO* gene are associated with variation in energy intake, but not energy expenditure. *Obesity* **16,** 1961–1965 (2008).
6. Gerken, T. *et al.* The obesity-associated *FTO* gene encodes a 2-oxoglutarate-dependent nucleic acid demethylase. *Science* **318,** 1469–1472 (2007).
7. Sanchez-Pulido, L. & Andrade-Navarro, M. A. The *FTO* (fat mass and obesity associated) gene codes for a novel member of the non-heme dioxygenase superfamily. *BMC Biochem.* **8,** 23 (2007).
8. Jia, G. *et al.* Oxidative demethylation of 3-methylthymine and 3-methyluracil in single-stranded DNA and RNA by mouse and human FTO. *FEBS Lett.* **582,** 3313–3319 (2008).
9. Trewick, S. C., Henshaw, T. F., Hausinger, R. P., Lindahl, T. & Sedgwick, B. Oxidative demethylation by *Escherichia coli* AlkB directly reverts DNA base damage. *Nature* **419,** 174–178 (2002).
10. Falnes, P. Ø., Johansen, R. F. & Seeberg, E. AlkB-mediated oxidative demethylation reverses DNA damage in *Escherichia coli*. *Nature* **419,** 178–182 (2002).
11. Westbye, M. P. *et al.* Human AlkB homolog 1 is a mitochondrial protein that demethylates 3-methylcytosine in DNA and RNA. *J. Biol. Chem.* **283,** 25046–25056 (2008).
12. Aas, P. A. *et al.* Human and bacterial oxidative demethylases repair alkylation damage in both RNA and DNA. *Nature* **421,** 859–863 (2003).
13. Duncan, T. *et al.* Reversal of DNA alkylation damage by two human dioxygenases. *Proc. Natl Acad. Sci. USA* **99,** 16660–16665 (2002).
14. Falnes, P. Ø. Repair of 3-methylthymine and 1-methylguanine lesions by bacterial and human AlkB proteins. *Nucleic Acids Res.* **32,** 6260–6267 (2004).
15. Ougland, R. *et al.* AlkB restores the biological function of mRNA and tRNA inactivated by chemical methylation. *Mol. Cell* **16,** 107–116 (2004).
16. Yu, B. *et al.* Crystal structures of catalytic complexes of the oxidative DNA/RNA repair enzyme AlkB. *Nature* **439,** 879–884 (2006).
17. Sundheim, O. *et al.* Human ABH3 structure and key residues for oxidative demethylation to reverse DNA/RNA damage. *EMBO J.* **25,** 3389–3397 (2006).
18. Yang, C. G. *et al.* Crystal structures of DNA/RNA repair enzymes AlkB and ABH2 bound to dsDNA. *Nature* **452,** 961–965 (2008).
19. Yu, B. & Hunt, J. F. Enzymological and structural studies of the mechanism of promiscuous substrate recognition by the oxidative DNA repair enzyme AlkB. *Proc. Natl Acad. Sci. USA* **106,** 14315–14320 (2009).
20. Koivisto, P., Duncan, T., Lindahl, T. & Sedgwick, B. Minimal methylated substrate and extended substrate range of *Escherichia coli* AlkB protein, a 1-methyladenine-DNA dioxygenase. *J. Biol. Chem.* **278,** 44348–44354 (2003).
21. Meyre, D. *et al.* Prevalence of loss-of-function *FTO* mutations in lean and obese individuals. *Diabetes* **59,** 311–318 (2010).
22. Boissel, S. *et al.* Loss-of-function mutation in the dioxygenase-encoding *FTO* gene causes severe growth retardation and multiple malformations. *Am. J. Hum. Genet.* **85,** 106–111 (2009).
23. Costas, M., Mehn, M. P., Jensen, M. P. & Que, L. Jr. Dioxygen activation at mononuclear nonheme iron active sites: enzymes, models, and intermediates. *Chem. Rev.* **104,** 939–986 (2004).
24. Sundheim, O., Talstad, V. A., Vagbo, C. B., Slupphaug, G. & Krokan, H. E. AlkB demethylases flip out in different ways. *DNA Repair* **7,** 1916–1923 (2008).
25. Mol, C. D. *et al.* Crystal structure and mutational analysis of human uracil-DNA glycosylase: structural basis for specificity and catalysis. *Cell* **80,** 869–878 (1995).
26. Slupphaug, G. *et al.* A nucleotide-flipping mechanism from the structure of human uracil-DNA glycosylase bound to DNA. *Nature* **384,** 87–92 (1996).
27. Nègre, D., Weitzmann, C. & Ofengand, J. *In vitro* methylation of *Escherichia coli* 16S ribosomal RNA and 30S ribosomes. *Proc. Natl Acad. Sci. USA* **86,** 4902–4906 (1989).
28. Micura, R. *et al.* Methylation of the nucleobases in RNA oligonucleotides mediates duplex-hairpin conversion. *Nucleic Acids Res.* **29,** 3997–4005 (2001).
29. Fan, J., Schnare, M. N. & Lee, R. W. Characterization of fragmented mitochondrial ribosomal RNAs of the colorless green alga *Polytomella parva*. *Nucleic Acids Res.* **31,** 769–778 (2003).
30. Klagsbrun, M. Differences in the methylation of transfer ribonucleic acid *in vitro* by the mitochondrial and cytoplasmic transfer ribonucleic acid methylases of HeLa cells. *J. Biol. Chem.* **248,** 2606–2611 (1973).

Supplementary Information is linked to the online version of the paper at www.nature.com/nature.

Acknowledgements We thank Y. Yamada at Photon Factory of Japan for assistance with data collection. This research was funded by Chinese Ministry of Science and Technology '863' grant no. 2008AA022305 and '973' grant no. 2006CB806704 to J. Chai, '863' grant no. 2008AA022317 to X.L. and the National Outstanding Young Scholar Science Foundation of National Natural Science Foundation of China grant no. 30825043 to J. Chang.

Author Contributions Z.H., T.N. and J. Chai designed the experiments. Experiments were performed by Z.H., T.N, J.B.C., X.L., M.Z., Q.W., W.C., J.W. and Y.F. Data were analysed by Z.H., T.N., X.L., J. Chai and J. Chang. J. Chai wrote the paper and Z.H. and X.L. contributed to editing the manuscript.

Author Information The atomic coordinates and structure factors of the FTOΔ31–3-meT complex have been deposited in the Protein Data Bank under accession code 3LFM. Reprints and permissions information is available at www.nature.com/reprints. The authors declare no competing financial interests. Correspondence and requests for materials should be addressed to J. Chai (chaijijie@nibs.ac.cn).

METHODS

Protein expression and purification. Wild-type and various mutants of human FTO were generated by standard PCR-based cloning strategy and their identities were confirmed by sequencing. All of the proteins were overexpressed in *E. coli* strain BL21 (DE3) using the vector **pET-15b** (Novagen). Cells expressing FTO were induced with 1 mM isopropyl β-D-1-thiogalactopyranoside (IPTG) for 12 h at room temperature. Cells were collected, pelleted and then resuspended in buffer A (50 mM Tris, pH 8.0, 100 mM NaCl). The cells were lysed by sonication and then centrifuged at 23,708*g* for 1 h. The soluble proteins were first purified using Ni^{2+}-resin (Novagen), and then further cleaned by ion-exchange (Source-15Q, Pharmacia) and gel-filtration (Superdex-200, Pharmacia) chromatography. All the protein purification was performed at 4 °C. For crystallization, the purified protein was concentrated to approximately 8 mg ml^{-1}.

Crystallization, data collection, structure determination and refinement. Crystals of the FTOΔ31–3-meT complex were generated by mixing the protein with an equal amount of well solution (2 μl) by the hanging-drop vapour-diffusion method. Both native and selenium-substituted FTOΔ31–3-meT complexes were crystallized in the buffer containing 10% (w/v) polyethylene glycol (PEG) 3350, 0.1 M tri-sodium citrate dehydrate, pH 5.6, 5 mM 3-meT and 3 mM NOG. The crystals belonged to space group *R*3 with one FTOΔ31–3-meT complex per asymmetric unit. For data collection, the crystals were equilibrated in a cryoprotectant buffer containing reservoir buffer plus 15.0% (v/v) glycerol. The native and selenium SAD data sets were collected at the Photon Factory at beamline NW12 using a CCD detector. All the data sets were processed using the program DENZO.

The ordered selenium sites were positioned by the program SOLVE. The experimental electron density calculated with the initial SAD phases and modified with the program RESOLVE was sufficient for manual model-building under the program O. All the residues of FTOΔ31 except 122–129, 160–188, 251–264, 424–426 and 499–505 were built into the electron density. The model was subsequently refined against the higher resolution data set (to 2.5 Å) with the program CNS. When justified by the electron density, Fe^{2+}, NOG and 3-meT were included in the structure refinement. Statistics of data collection, phasing and structure refinement are given in Supplementary Table 1.

Gel-filtration assay. The human complementary DNAs of *FTO* encoding residues 1–326 and 327–505 were subcloned into **pET-15b** (Novagen, with an N-terminal His tag) and **pET-30a** (Novagen, without tag), respectively, and co-expressed in *E. coli* strain BL21(DE3). The soluble fraction was purified using an affinity column and further cleaned by an anion-exchange column. The proteins thus purified were subjected to gel filtration analysis (Superdex-200, Pharmacia). The protein purification was performed at 4 °C. Aliquots of the fractions corresponding to the peak were visualized by Coomassie staining after SDS–PAGE.

***In vitro* demethylation activity assay.** The general procedure used for the enzymatic activity assay was described previously[6,8]. For a typical reaction, 2 μl 3-meT (1.0 mg ml^{-1}) and 2 μl human FTO wild-type or mutant proteins (5.0 mg ml^{-1}) were incubated in 100 μl of reaction buffer at 16 °C for 12 h. The reaction buffer contained 50 mM 2-(*N*-morpholino) ethanesulphonic acid (MES), pH 6.0, 0.5 mM $(NH_4)_2FeSO_4$, 1 mM 2-ketoglutarate and 2 mM ascorbic acid. The reaction was stopped by the addition of EDTA to 5 mM and the internal standard BrdU was subsequently added to the reaction mixture to a final concentration of 0.065 mM. The samples were analysed by LC–MS on a Waters Auto Purification LC/MS system (3100 Mass Detector, 2545 Binary Gradient Module, 2767 Sample Manager, and 2998 Photodiode Array (PDA) Detector). The system was equipped with a Waters C18 5μm SunFire separation column (150 × 4.6 mm), equilibrated with HPLC grade water (solvent A) and HPLC grade methanol (solvent B) at a 90:10 (v/v) ratio with a flow rate of 1.0 ml min^{-1} at room temperature. The eluent was a mixture of A and B with a linear gradient: 90% A/10% B→20% A/80% B (6 min)→0% A/100% B (0.2 min)→0% A/100% B (5.8 min). The detection wavelength was set at 266 nm. The structural identification of the starting material and demethylated product was established by mass spectrometry (3100 Mass Detector) using both positive- and negative-ion modes.